Synthesis and Characterization of a Polyfluorene Containing Carbazole and Oxadiazole Dipolar Pendent Groups and Its Application to Electroluminescent Devices

MAO-CHUAN YUAN, PING-I SHIH, CHEN-HAN CHIEN, CHING-FONG SHU

Department of Applied Chemistry, National Chiao Tung University, Taiwan, Republic of China

ABSTRACT: We have synthesized a blue-light-emitting polyfluorene (PF) derivative (**PF-CBZ-OXD**) that presents bulky hole-transporting carbazole and electron-transporting oxadiazole pendent groups functionalized at the C-9 positions of alternating fluorene units. The results from photoluminescence and electrochemical measurements indicate that both the side chains and the PF main chain retain their own electronic characteristics in the copolymer. An electroluminescent device incorporating this polymer as the emitting layer was turned on at 4.5 V; it exhibited a stable blue emission with a maximum external quantum efficiency of 1.1%. Moreover, we doped **PF-CBZ-OXD** and its analogue **PF-TPA-OXD** with a red-light-emitting iridium phosphor for use as components of phosphorescent red-light emitters to investigate the effect of the host's HOMO energy level on the degree of charge trapping and on the electrophosphorescent efficiency. We found that spectral overlap and individual energy level matching between the host and guest were both crucial features affecting the performance of the electroluminescence devices. Atomic force microscopy measurements indicated that the dipolar nature of **PF-CBZ-OXD**, in contrast to the general nonpolarity of polydialkylfluorenes, provided a stabilizing environment that allowed homogeneous dispersion of the polar iridium triplet dopant. © 2007 Wiley Periodicals, Inc. J Polym Sci Part A: Polym Chem 45: 2925–2937, 2007
Keywords: atomic force microscopy; charge transport; conjugated polymers; light-emitting diodes

INTRODUCTION

The feasibility of utilizing low-cost solution processes for the preparation large-area display devices makes polymeric materials very attractive for use as active components in such applications as flat-panel displays and solid state lighting.[1] Electroluminescent polymers that have sufficiently large band gaps such that they emit blue light efficiently are of particular interest because they can be used either as blue light sources in full-color displays or as host materials for lower-energy fluorescent or phosphorescent dyes.[2–10] Because of their high photoluminescence (PL) and electroluminescence (EL) efficiencies and thermal stabilities, polyfluorenes (PFs) are very promising candidates for use as such blue-light-emitting materials.[11–14] In addition, the facile functionalization at the C-9 position of the fluorene unit provides the opportunity to improve both the solubility and processability of the PFs, while also offering the ability to tune their optoelectronic properties.[9,15–21] Moreover, PFs may be readily color-tuned through chemical incorporation with low-bandgap

comonomers or through physical doping with lower-energy fluorescent and/or phosphorescent dyes.[2–10,22–38] Consequently, PFs can function as both the host and the blue emitter in white-light-emitting devices.[39–44]

Triarylamines have emerged as an attractive class of hole injecting/transporting materials for use in organic light-emitting diodes because of their relatively low ionization potentials and high mobilities.[45] Müllen and coworkers first introduced triphenylamino groups into PFs as side chains.[15] Subsequently, we reported a highly efficient blue-light-emitting PF derivative **PF-TPA-OXD** that featured both hole-transporting triphenylamine (**TPA**) units and electron-transporting oxadiazole (**OXD**) moieties functionalized at the C-9 positions of fluorene moieties.[17] These bulky bipolar pendent groups provided two functions simultaneously: suppressing aggregate/excimer formation and improving charge injection/transportation. This blue fluorene-based copolymer is also a very promising host material for use in molecularly doped electrophosphorescence devices because of its wide energy gap and large number of charge-transporting pendent groups, which provide improved confinement of triplet excitons in the phosphorescent dopants and more-balanced charge transportation, respectively.[7]

Carbazoles (**CBZ**s) are another well-established group of hole-transporting materials[46–48] They have been incorporated into the main chains, or attached to the side chains, of light-emitting polymers to improve their hole injection and transpor-

tation properties.[34,49–53] Herein, we report the synthesis, characterization, and device performance of a new statistical bipolar copolymer **PF-CBZ-OXD** bearing hole-transporting **CBZ** units together with electron-transporting **OXD** pendent groups at the C-9 positions of fluorene moieties. For most **CBZ**-substituted PFs, the pendent groups have been attached to the main chains through a long alkyl chains; **PF-CBZ-OXD** represents the first example of a fluorene-based copolymer containing **CBZ** units functionalized directly at the C-9 positions of fluorene moieties. Moreover, we used this copolymer and **PF-TPA-OXD** as host materials for a red-light-emitting iridium complex, and have investigated the effect of the host's HOMO energy level on the degree of charge trapping and on the electrophosphorescent efficiency. We have found that spectral overlap and individual energy level matching between the host and guest are both crucial features affecting the performance of EL device; hole trapping in the guest and subsequent recombination with an electron injected from the metal electrode requires a sufficiently higher oxidation potential for the host than for the guest.
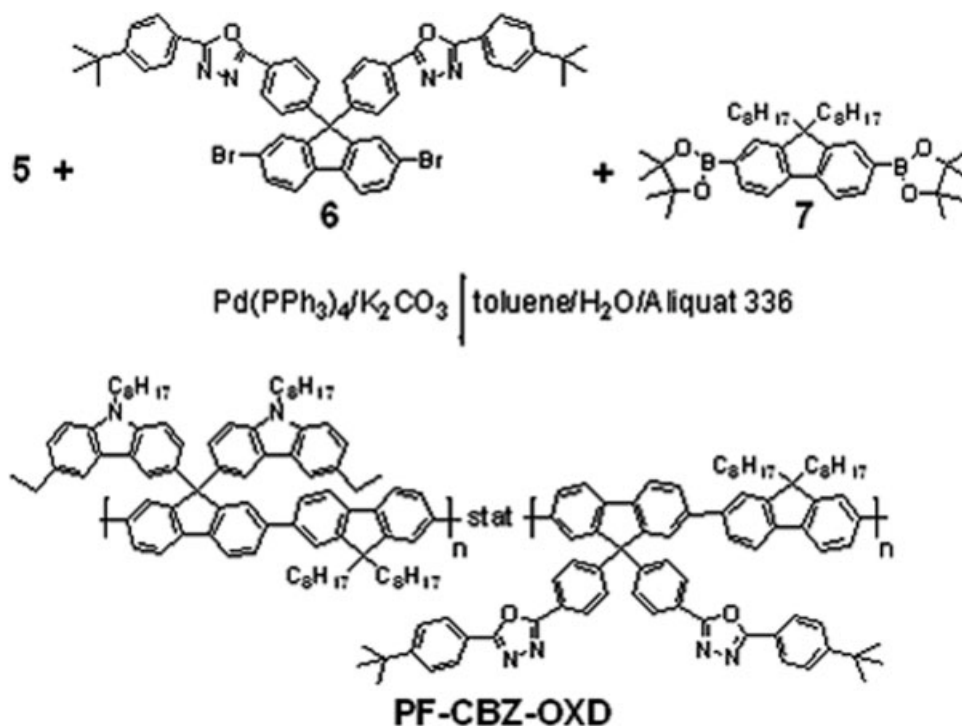
RESULTS AND DISCUSSION

Polymer Synthesis and Characterization

Scheme 1 illustrates the synthetic route followed for the preparation of the dibromo monomer **5**.
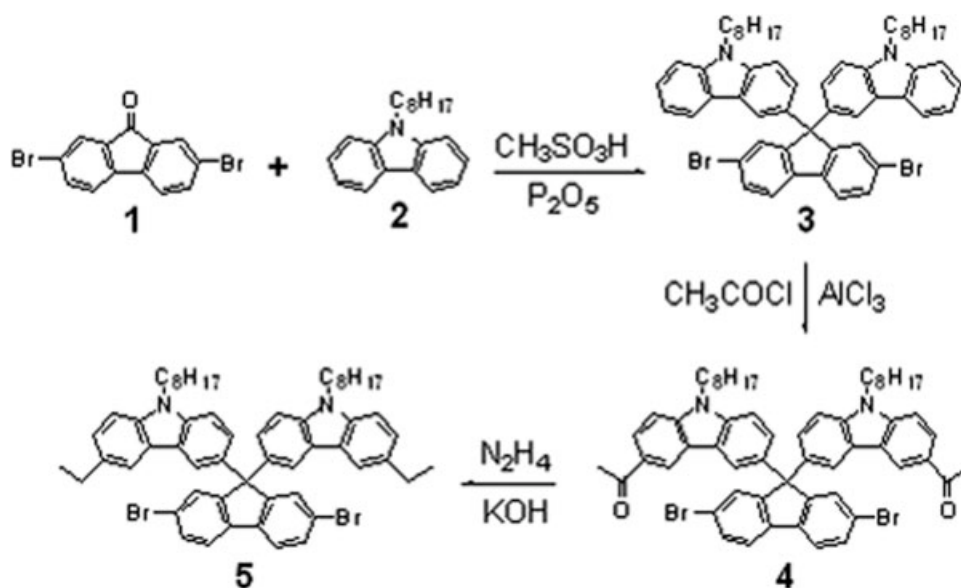
Scheme 1. Synthesis of monomer **5**.

Scheme 2. Synthesis of **PF-CBZ-OXD** copolymer.

The acid-promoted condensation reaction between 2,7-dibromofluorenone (**1**) and 9-octyl-CBZ (**2**) gave the CBZ/fluorene hybrid **3**. This method resembles a procedure that we used recently to introduce N-phenylcarbazole groups onto the C-9 position of fluorene.[54] Subsequent Friedel-Crafts acylation of **3** with acetyl chloride yielded compound **4**, on which the acetyl groups were reduced to ethyl groups through Wolff-Kishner reduction with NH_2NH_2/KOH to furnish the desired dibromo monomer **5**, containing two 3-ethyl-9-octylcarbazol-6-yl moieties substituted at the C-9 position of 2,7-dibromofluorene. Previous reports have indicated that CBZ derivatives undergo oxidative C—C couplings at the 3- and 6-positions of the CBZ ring.[55] We hoped that the introduction of 3,6-disubstituted CBZs into the monomer **5** would block the electrochemically active sites of the CBZ ring to give the resultant polymer additional electrochemical stability.

As indicated in Scheme 2, the statistical PF copolymer **PF-CBZ-OXD**, which possessed bulky hole-transporting **CBZ** and electron-transporting **OXD** pendent groups at the C-9 positions its fluorene units, was synthesized through Suzuki coupling of the dibromides **5** and **6** with the diboronate **7** at a mole ratio of 1.0:1.0:2.0. This copolymerization was performed using $Pd(PPh_3)_4$ as the

catalyst in a mixture of toluene and aqueous K_2CO_3 (2.0 M) in the presence of Aliquat 336 as a phase transfer reagent. After the polymerization process was complete, the end groups of the polymer chains were capped through sequential reactions with phenylboronic acid and bromobenzene, each under reflux for 12 h. The structure of the resultant copolymer was confirmed by ^{1}H and ^{13}C NMR spectroscopy. In the ^{13}C NMR spectrum, we observe signals at δ 65.8, 66.0, and 55.3 that correspond to the C-9 carbon atoms of the three different fluorene units in **PF-CBZ-OXD**. These signals are almost superimposed with the signals of the C-9 carbon atoms of the monomers **5**, **6**, and **7**.

Because of the presence of solubilizing n-octyl chains in the CBZ pendent groups and fluorene units, **PF-CBZ-OXD** dissolves readily in common organic solvents, such as toluene, chloroform, dichloromethane, chlorobenzene, and THF. The molecular weight of this polymer was determined using size exclusion chromatography (SEC; eluent: THF), calibrating against polystyrene standards. The polymer possesses a number-average molecular weight (M_n) of 1.6×10^4 g/mol, with a polydispersity index of 1.8. We investigated the thermal properties of **PF-CBZ-OXD** by performing differential scanning calorimetry (DSC) and thermogravimetric analysis
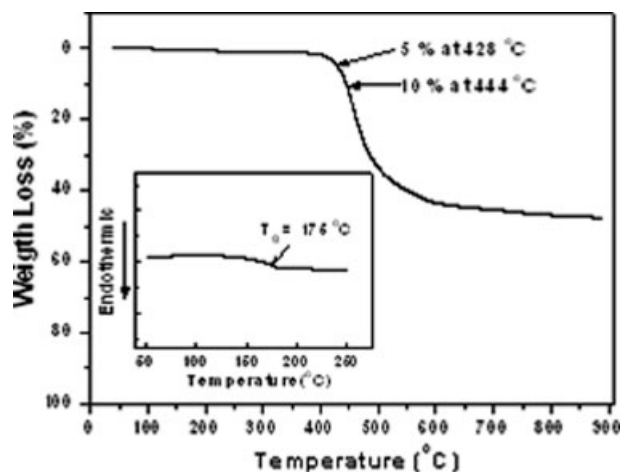
Figure 1. TGA trace of **PF-CBZ-OXD** recorded at a heating rate 10 °C/min. Inset: DSC trace recorded at a heating rate of 20 °C/min.

(TGA). In the DSC measurement, a distinct glass transition was observed at 175 °C (see the inset of Fig. 1), which is much higher than that of poly(9,9-dioctylfluorene) (**POF**; $T_g = \sim 67$ °C).[56] In addition, the value of T_g of **PF-CBZ-OXD** is slightly higher than that of a bipolar fluorene co-polymer **PF-TPA-OXD** ($T_g = 166$ °C).[17] It is evident that the presence of rigid CBZ and oxadiazole groups at the C9 positions of the fluorene repeating units provided a sterically bulky structure that enhanced the chain rigidity of **PF-CBZ-OXD** and restricted its segmental mobility, resulting in its much higher value of T_g. Such a high value of T_g, which could prevent morphological change and suppress the formation of aggregates and excimers upon exposure to heat, is desirable for polymers that are to be used as emissive materials for light-emitting applications. As revealed by TGA (Fig. 1), **PF-CBZ-OXD** exhibited excellent thermal stability; its 5 and 10% weight losses occurred at 428 and 444 °C, respectively.

Photophysical Properties

We measured the optical properties of **PF-CBZ-OXD** both in dilute solution and in the solid state; Figure 2 presents these spectra and Table 1 summarizes the spectral data. In chloroform solution, **PF-CBZ-OXD** exhibits a main absorption peak at 392 nm and a shorter-wavelength absorption at ~ 300 nm. From a comparison of this spectrum with the absorption spectra of **POF**, 9-octylcarbazole, and 2,5-di(4-*tert*-butyl-

phenyl)-1,3,4-oxadiazole (*t*-BuOXD), we ascribe the band at 392 nm to a π-π* transition derived from the conjugated PF backbone and we assign the band at ~ 300 nm to the combined absorptions of the **CBZ** and **OXD** pendent groups. Upon excitation of the polymer main chain at 392 nm, the emission spectrum displays a vibronic fine structure with two sharp bands at 421 and 444 nm, which are nearly identical to the characteristic emission bands obtained from **POF** ($\lambda_{max} = 418, 442$ nm). This result suggests that the incorporation of bulky **CBZ** and **OXD** groups onto fluorene units via their C-9 carbon atoms does not perturb the conjugation of the main chain. Upon irradiation at 300 nm, the blue fluorescence **PF-CBZ-OXD** was identical to that under excitation of the POF backbone at 390 nm, we could not detect any luminescence at ~ 360 nm arising from the side chains. The fact that we observed complete quenching of the side chain emissions-even in a very dilute solu-
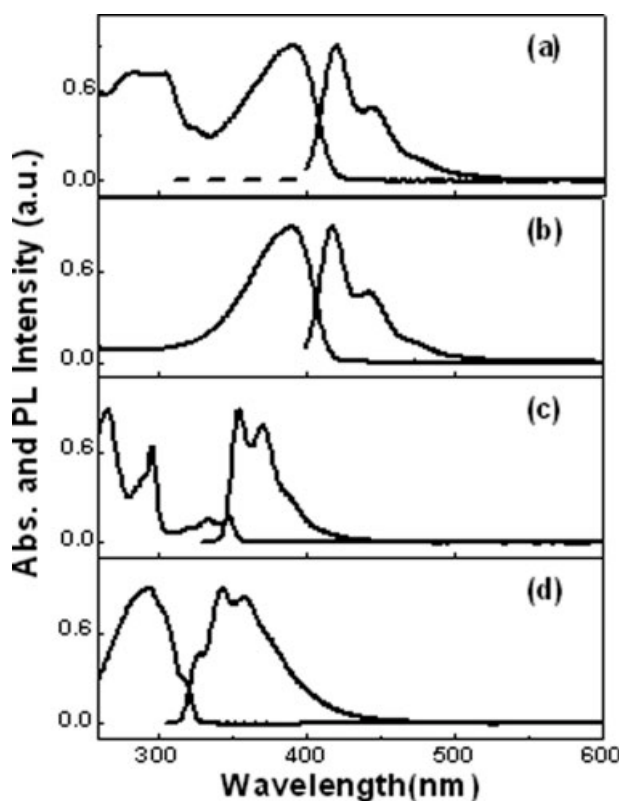

Figure 2. UV–vis absorption and PL spectra of (a) **PF-CBZ-OXD** (excited at 390 nm), (b) **POF** (excited at 390 nm), (c) 9-octylcarbazole (excited at 333 nm), and (d) *t*-BuOXD (excited at 300 nm) in dilute chloroform solutions. The PL spectrum of **PF-CBZ-OXD** excited at 300 nm (dashed line) is also included in (a).

Table 1. Optical Properties of PF-CBZ-OXD, POF, 9-Octyl-carbazole, and *t*-BuOXD

	Absorption, λ_{max} (nm)		PL, λ_{max} (nm)		
	Solution[a]	Film[b]	Solution[a]	Film[b]	Φ_f^{ac}
PF-CBZ-OXD	300, 392	306, 390	421, 444	428, 451	1.0
POF	389	390	418, 442	424, 448	0.83
9-octyl-carbazole	296, 333, 348		370, 386		
t-BuOXD	294		344, 358		

[a] In chloroform.
[b] Spin-coated from their $CHCl_3$ solutions.
[c] The relative quantum yield was measured with reference to 9,10-diphenylanthracene in toluene ($\Phi = 0.90$).

tion (10^{-8} M)-indicates that efficient intrachain energy transfer occurred in the **PF-CBZ-OXD** copolymer as a result of good spectral overlap between the emission spectrum of the pendent groups and the absorption spectrum of the PF backbone (Fig. 2). In addition, these pendent groups and the π-conjugated backbone were connected through a common tetrasubstituted carbon atom (C9); the close distance between the donor and acceptor may also account for the highly efficient energy transfer. Consequently, most excitons that formed in the **CBZ** and **OXD** side chains through direct photoexcitation were likely to migrate to the lower-energy main chain, from which emission occurred. The PL quantum yield in toluene when excited at 365 nm was 1.0, measured relative to 9,10-diphenylanthrancene ($\Phi_f = 0.9$) as a standard.[57] In comparison to the behavior in dilute solution, the absorption spectrum of a film that had been spin-coated onto a quartz substrate was slightly broadened, while the emission spectrum displayed a red-shift of 7 nm with maxima at 428 and 451 nm.

Electrochemical Studies

We employed cyclic voltammetry to investigate the redox behavior of **PF-CBZ-OXD** and to estimate its HOMO and LUMO energy levels. The electrochemical processes of this polymer film coated on a glassy carbon electrode were monitored in a standard three-electrode electrochemical cell using ferrocene as the internal standard in an electrolyte of 0.1 M tetrabutylammonium hexafluorophosphate ($TBAPF_6$) in acetonitrile at a scanning rate of 50 mV/s. On the basis of the onset potentials of the oxidation and reduction,

which were 0.79 and -2.32 V, respectively, we estimated the HOMO and LUMO energy levels of **PF-CBZ-OXD** to be -5.59 and -2.48 eV, respectively, with regard to the energy level of ferrocene (4.8 eV below vacuum). The high-lying HOMO level may originate from the electron-rich nature of the **CBZ** moiety; it is in agreement with the data reported previously for PF copolymers containing CBZ side chain (values from -5.58 to -5.61 eV).[52] At the same time, we attribute the low-lying LUMO level to the electron-deficient nature of the pendent **OXD** units; its value is similar to that reported for an **OXD**-substituted PF (-2.47 eV).[17] In comparison with **PF-TPA-OXD**, for which the HOMO level occurs at -5.30 eV, the replacement of the **TPA** units with **CBZ** moieties decreases the HOMO level of **PF-CBZ-OXD** markedly (to -5.59 eV). It is noteworthy that this lower-lying HOMO level significantly facilitated hole trapping at electrophosphorescent iridium dopants when the **CBZ** copolymer was employed as the host emitting material; consequently, we observed efficient electrophosphorescence (*vide infra*).

EL Properties of LED Devices

To evaluate the potential use of **PF-CBZ-OXD** as a blue emissive material in polymer LED applications, we fabricated a blue-emitting device having the configuration ITO/PEDOT (35 nm)/**PF-CBZ-OXD** (50–70 nm)/TPBI (30 nm)/Mg:Ag (100 nm)/Ag (100 nm). The PEDOT layer was used as a hole injection layer to facilitate hole conduction, and also to smoothen the relatively rough ITO layer; the TPBI layer, deposited through thermal evaporation, was employed as an electron-transporting and hole-blocking layer. As indicated in
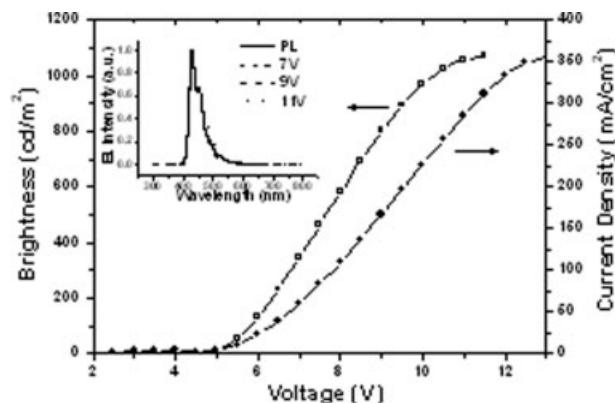
Figure 3. Current density–voltage–luminance characteristics of ITO/PEDOT/**PF-CBZ-OXD**/TPBI/Mg:Ag. Inset: PL spectrum and corresponding EL spectra recorded at different applied voltages.

the inset of Figure 3, this device emitted a deep-blue color-with two sharp bands at 428 and 452 nm in the EL spectrum-corresponding to CIE color coordinates of (0.16, 0.06) at 7 V. These features in the EL spectrum are nearly identical, with respect to their position and shape, to those in the solid state PL spectrum mentioned above, indicating that both the PL and EL originate from the same radiative decay process of singlet excitons. Unlike devices constructed from polydialkylfluorenes, which exhibit an undesirable emission band between 500 and 600 nm resulting from keto defects, aggregation, and/or excimer formation,[58–60] the device based on **PF-CBZ-OXD** exhibited a voltage-independent and stable

EL spectrum. There was no significant change in the appearance of the EL spectra upon increasing the applied voltage from 7 to 11 V (i.e., potential near to that required to achieve maximum brightness). Figure 3 displays the current–voltage (I-V) and luminance–voltage (L-V) characteristics of the device turned on at 4.5 V (corresponding to 1 cd/m^2); the maximum external quantum efficiency was 1.1% at 17.6 mA/cm^2, which was superior to that of polydialkylfluorene and comparable to those of other PF derivatives.[16,17,61,62] In addition, a reference device with the same device configuration using **POF** as the light-emitting material also exhibited inferior performance, with the maximum external quantum efficiency of 0.78%.[63] Table 2 summaries the performance of this **PF-CBZ-OXD**-based device; further improvements may be possible after optimizing the device structure.

PF-CBZ-OXD as a Host Material in a Red-Light-Emitting Electrophosphorescent Device

The bipolar PF derivative **PF-TPA-OXD** has been used extensively as a host material for the fabrication of electrophosphorescent polymer LEDs,[5–7] mainly because of its improved hole- and electron-transporting capabilities. In this study, we employed the novel bipolar PF derivative **PF-CBZ-OXD**, which possesses hole-transporting **CBZ** and electron-transporting **OXD** side chains, as a polymeric host doped with the red-light-emitting phosphorescent dye

Table 2. Performances of Devices Having the Structure ITO/PEDOT/Polymer Emitting Layer/TPBI/Mg:Ag

	PF-CBZ-OXD	PF-CBZ-OXD: Ir(FPQ)$_2$(acac)	PF-TPA-OXD: Ir(FPQ)$_2$(acac)
Turn-on voltage (V)[a]	4.5	5.6	4.2
Voltage (V)[b]	5.9 (7.8)	10.3 (13.0)	8.3 (10.9)
Brightness (cd/m^2)[b]	111 (540)	1760 (7380)	1020 (4050)
Luminance efficiency (cd/A)[b]	0.55 (0.54)	8.8 (7.4)	5.1 (4.1)
External quantum efficiency (%)[b]	1.00 (1.00)	8.6 (7.2)	4.8 (3.8)
Maximum brightness (cd/m^2)	1070 (at 11)	8630 (at 14 V)	5490 (at 13 V)
Maximum luminance efficiency (cd/A)	0.58	8.8	5.2
Maximum external quantum efficiency (%)	1.1	8.6	4.8
EL maximum (nm)[c]	430	632	624
CIE coordinates, x and y[c]	0.16 and 0.06	0.67 and 0.32	0.48 and 0.23

[a] Recorded at 1 cd/m^2.
[b] Recorded at 20 mA/cm^2, data in parentheses were recorded at 100 mA/cm^2.
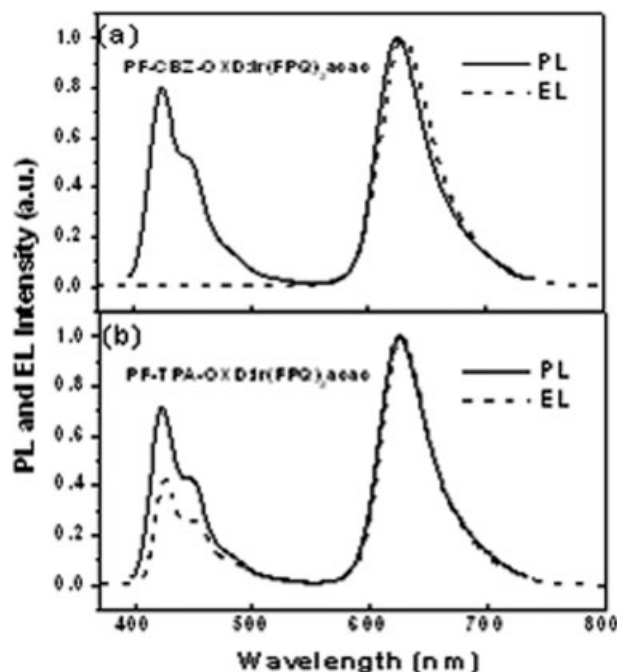[c] Recorded at 7 V.

Figure 4. PL and EL spectra of (a) **PF-CBZ-OXD** and (b) **PF-TPA-OXD**, both doped with 1.1 mol % **Ir(FPQ)$_2$(acac)**.

Ir(FPQ)$_2$(acac) to realized an efficient phosphorescent polymer light-emitting diode (PLEDs). The device architecture was ITO/PEDOT (35 nm)/ **PF-CBZ-OXD**:1.1 mol % of **Ir(FPQ)$_2$(acac)** (50–70 nm)/TPBI (30 nm)/Mg:Ag (100 nm)/Ag (100 nm). To investigate the effect of the HOMO level of the host material on the device efficiency, we also fabricated a control device in which we replaced **PF-CBZ-OXD** with **PF-TPA-OXD** as the host material at the same doping concentration. Figure 4(a) depicts the PL and EL spectra of the **PF-CBZ-OXD:Ir(FPQ)$_2$(acac)** device. The PL profile contains two components: the one occurring at $\sim$ 426 nm is a characteristic emission of the **PF-CBZ-OXD** host; the other at $\sim$623 nm corresponds to the triplet emission of **Ir(FPQ)$_2$(acac)**.[64] In contrast, the corresponding EL spectrum is completely dominated by the dopant emission, i.e., a saturated-red triplet emission from the Ir-complex. The dramatic difference between the PL and EL spectra reveals that Förster energy transfer of an exciton from the host to the dopant does not account solely for the observed EL. Another dominant mechanism for exciting **Ir(FPQ)$_2$(acac)** would be direct charge trapping at the dopant sites, followed by recombination with opposite charges.[7,65,66] On the other hand, the PL and EL spectra of the **PF-TPA-OXD:Ir(FPQ)$_2$(acac)** blends are quite similar in terms of their

shape and position [Fig. 4(b)], indicating that energy transfer remained as the main operating mechanism in the EL process.

According to the energy level diagram (Fig. 5), the HOMO level of **PF-CBZ-OXD** occurs at -5.6 eV, which is lower than that of **PF-TPA-OXD** (-5.3 eV); this subtle change in the HOMO level energy has a major impact on both the current density and EL efficiency. In the case of the **PF-CBZ-OXD:Ir(FPQ)$_2$(acac)** blend, the ionization potential of **Ir(FPQ)$_2$(acac)** is 0.6 eV below the HOMO level of **PF-CBZ-OXD**; therefore, holes can be trapped efficiently at the guest and subsequently they can recombine with opposite charges (electrons) to form excitons. Upon switching the host to **PF-TPA-OXD**, **Ir(FPQ)$_2$(acac)** becomes a much less effective trap site for holes because of the shallow trap (depth: 0.3 eV) constructed by **Ir(FPQ)$_2$(acac)** in the **PF-TPA-OXD** host. Once the holes are trapped at the HOMO of **Ir(FPQ)$_2$(acac)**, there is a high possibility that they may detrap and hop back to the HOMOs of the TPA moieties by overcoming this smaller energy barrier; as a result, the excitons eventually reform at the host.[7] Thus, most of excitons still form at the host under the influence of the electric field; subsequent energy transfer to the dopant contributes to the triplet emission in a manner similar to that which we observed in the PL spectra.

Figure 6 displays the current density versus voltage (*I-V*) characteristics of **Ir(FPQ)$_2$(acac)**-doped devices that employ **PF-CBZ-OXD** and **PF-TPA-OXD** as host materials, respectively. It is apparent that the operating voltage of the **PF-CBZ-OXD**-based devices was higher than that of the **PF-TPA-OXD** device. This result is consistent with the charge trapping mechanism proposed previously for the **PF-CBZ-OXD** device. Figure 7 presents the EL performances of these two devices; Table 2 summarizes the data. The maximum external quantum efficiency of **PF-CBZ-OXD**-blend reached as high as 8.6% (8.8 cd/A) at 23.0 mA/cm^2; conversely, the **PF-TPA-OXD**-blend, which does not feature an efficient charge trapping mechanism in its EL process, exhibited a relatively poor performance. Moreover, the **PF-CBZ-OXD**-based device exhibited a satisfying saturated red emission that was located precisely at the standard red region (0.67, 0.32) of the CIE diagram for the National Television Systems Committee (NTSC) color system.

Phase separation processes in host–guest blends may affect their EL performance. To
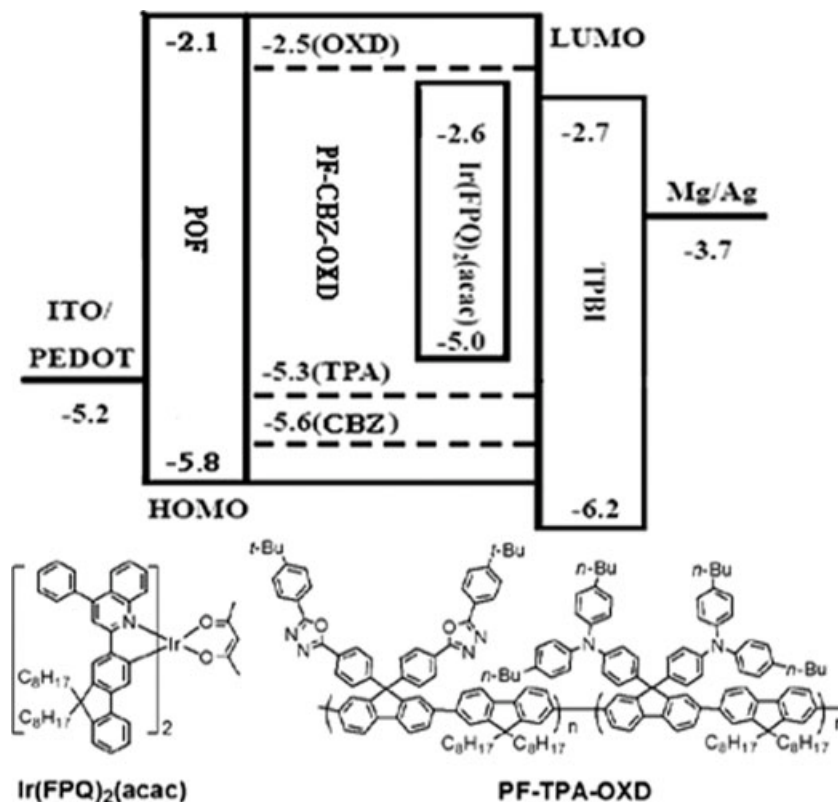
Figure 5. Energy diagram (in eV) for materials involved in EL devices having the configuration ITO/PEDOT/polymer/TPBI/Mg:Ag. The chemical structures of **PF-TPA-OXD** and **Ir(FPQ)₂(acac)** are provided.

investigate the effects of the **CBZ** and **OXD** pendent groups on the degree of dispersion of the polar organometallic triplet dopant in the polymeric host, we used atomic force microscopy (AFM) to investigate the phase morphology of the **PF-CBZ-OXD**:**Ir(FPQ)₂(acac)** blend. For the sake of comparison, we also prepared a **POF : Ir(FPQ)₂(acac)** blend. Figure 8 displays
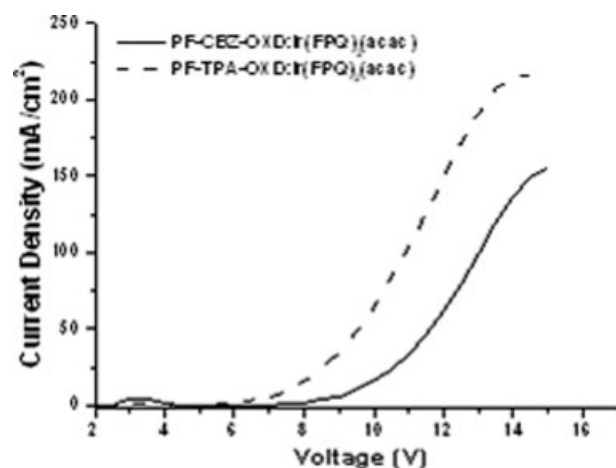

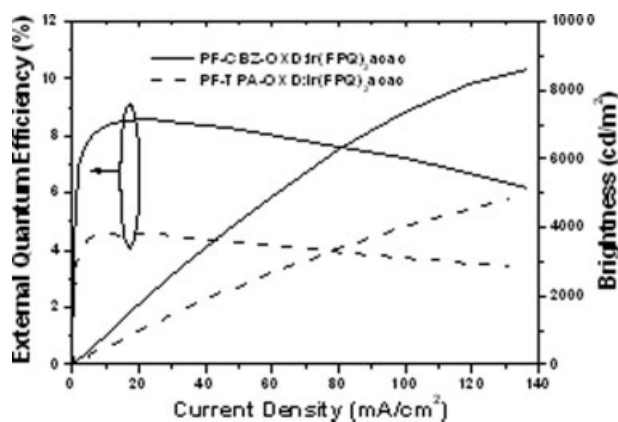**Figure 6.** Plots of current density versus voltage of 1.1 mol % **Ir(FPQ)₂(acac)**-doped devices.

Figure 7. Plots of external quantum efficiency and brightness versus current density of **Ir(FPQ)₂(acac)**-doped devices.
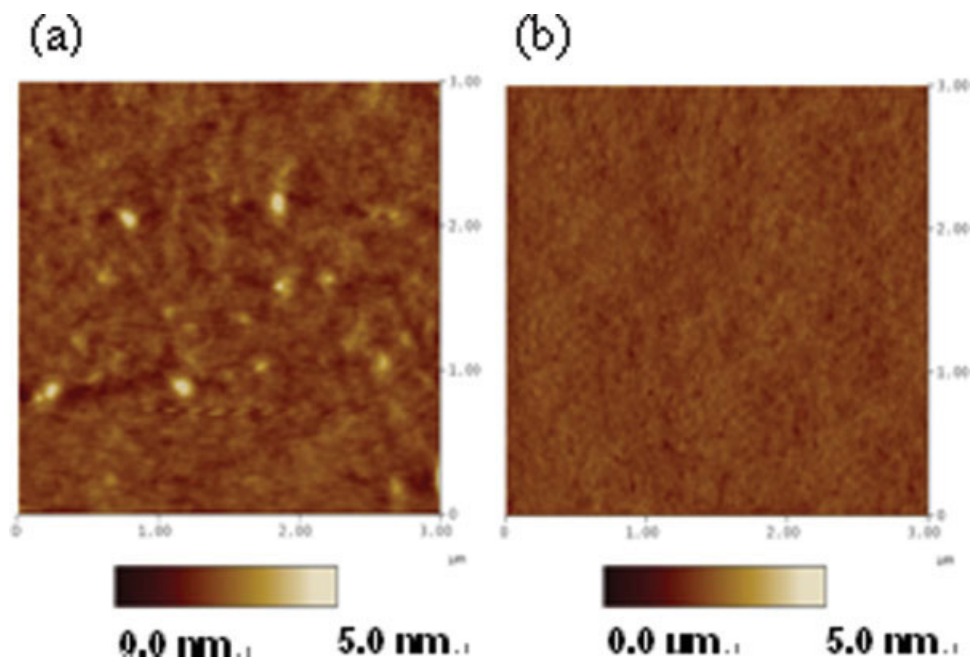
Figure 8. AFM images (tapping mode) of (a) **POF** and (b) **PF-CBZ-OXD**, both doped with 1.1 mol % **Ir(FPQ)₂(acac)**. [Color figure can be viewed in the online issue, which is available at www.interscience.wiley.com.]

the surface topographies of the spin-coated films. The doped **PF-CBZ-OXD** film was smooth and featureless with a root-mean-square (RMS) surface roughness of 0.35 nm, revealing that the film was homogeneous with no phase separation or aggregation. In contrast, the doped **POF** film displayed the some hill-like structures and possessed a higher surface roughness (0.55 nm), suggesting the formation of aggregates. These results indicate that the dipolar **PF-CBZ-OXD**, in contrast to the nonpolar **POF**, provides a compatible environment for the iridium complex and, consequently, it prevents the formation of aggregates.

CONCLUSIONS

We have synthesized a thermally stable blue-light-emitting polymer, **PF-CBZ-OXD**, which contains bulky hole-transporting **CBZ** and electron-transporting **OXD** pendent groups at the C-9 positions of alternating fluorene units. A light-emitting diode device prepared using **PF-CBZ-OXD** as the emitting layer exhibited an efficient, stable, blue-light emission; its turn-on voltage was 4.5 V and its maximum external quantum efficiency was 1.1%. To investigate the effect of the host's HOMO energy level on the degree of charge trapping and on the electrophosphorescence efficiency, we doped **PF-CBZ-OXD** and its analogue, **PF-TPA-OXD**, with an iridium phosphor, **Ir(FPQ)₂(acac)**, for use as components of phosphorescent red-light emitters in PLEDs. We found that spectral overlap and individual energy level matching between the host and guest are both crucial features affecting the performance of these EL devices. The HOMO energy level of **PF-CBZ-OXD** (−5.6 eV) was lower than that of **PF-TPA-OXD** (−5.3 eV); this subtle change in the HOMO energy level has a major impact on both the current density and EL efficiency. Consequently, the maximum external quantum efficiency of the **PF-CBZ-OXD** blend reached as high as 8.6% (8.8 cd/A) at 23.0 mA/cm² ; conversely, the **PF-TPA-OXD** blend, which did not feature an efficient charge trapping mechanism in its EL process, exhibited relatively poor performance.

EXPERIMENTAL

Materials

2,7-Dibromofluorenone (**1**),[67] and 9-octyl-CBZ (**2**),[55] the monomers **6** and **7**,[16,68] **Ir(FPQ)₂(acac)**,[64]

and **PF-TPA-OXD**[17] were prepared according to reported procedures. Solvents were dried using standard procedures. All other reagents were used as received from commercial sources, unless otherwise stated.

Characterization

^{1}H and ^{13}C NMR spectra were recorded on a Bruker-DRX 300 (300 MHz) spectrometer. Mass spectra were obtained using a JEOL JMS-HX 110 mass spectrometer. Size exclusion chromatography (SEC) was performed using a Waters chromatography unit interfaced with a Waters 410 differential refractometer; three 5-μm Waters styragel columns (300 × 7.8 mm^2) were connected in series in order of decreasing pore size (10^4, 10^3, and 10^2 Å); THF was the eluent. Standard polystyrene samples were used for calibration. Differential scanning calorimetry (DSC) was performed using a SEIKO EXSTAR 6000DSC unit operated at heating and cooling rates of 20 and 40 °C/min, respectively. Samples were scanned from 30 to 250 °C, cooled to 0 °C, and then scanned again from 30 to 250 °C. The glass transition temperatures (T_g) were determined from the second heating scans. Thermogravimetric analysis (TGA) was undertaken using a Perkin-Elmer TGA Pyris 1 instrument. The thermal stabilities of the samples were determined under a nitrogen atmosphere by measuring their weight losses while heating at a rate of 20 °C/min. UV–vis spectra were measured using an HP 8453 diode-array spectrophotometer. PL spectra were obtained using a Hitachi F-4500 luminescence spectrometer. Cyclic voltammetry measurements were performed using a BAS 100 B/W electrochemical analyzer operated at a scan rate of 50 mV/s; the solvent was anhydrous acetonitrile and 0.1 M tetrabutylammonium hexafluorophosphate (TBAPF$_6$) was the supporting electrolyte. The potentials were measured against an Ag/Ag$^+$ (0.01 M AgNO$_3$) reference electrode; ferrocene was the internal standard. The onset potentials were determined from the intersection of two tangents drawn at the rising and background currents of the cyclic voltammogram. Atomic force microscopy measurements were undertaken in the tapping mode using a Digital Nanoscope IIIa instrument under ambient conditions.

2,7-Dibromo-9,9-bis(9-octylcarbazol-3-yl)-fluorene (3)

Eaton's reagent (7.7 wt % P$_2$O$_5$ in CH$_3$SO$_3$H, 2.0 mL) was added to a solution of **1** (2.42 g, 7.14 mmol) and **2** (4.38 g, 15.7 mmol) in CH$_2$Cl$_2$ (20

mL), which was then stirred under nitrogen and heated under reflux for 2 h. The cooled mixture was diluted with CH$_2$Cl$_2$ and washed with aqueous sodium bicarbonate. The organic phase was dried (MgSO$_4$) and concentrated under reduced pressure. The crude product was purified by column chromatography, eluting with CH$_2$Cl$_2$/hexane (1:8), followed by recrystallization from cyclohexane to afford **3** (2.10 g, 33.4%) as white crystals. ^{1}H NMR (300 MHz, CDCl$_3$): δ 0.86 (t, J = 6.6 Hz, 6H), 1.25–1.40 (m, 20H), 1.84–1.88 (m, 4H), 4.26 (t, J = 7.4 Hz, 4H), 7.15 (td, J = 7.4, 0.9 Hz, 2H), 7.29 (d, J = 9.0 Hz, 2H), 7.33 (dd, J = 8.7, 1.5 Hz, 2H), 7.37 (d, J = 8.1 Hz, 2H), 7.43 (td, J = 7.4, 0.9 Hz, 2H), 7.50 (dd, J = 8.1, 1.5 Hz, 2H), 7.64–7.66 (m, 4H), 7.92–7.95 (m, 4H). ^{13}C NMR (75 MHz, CDCl$_3$): δ 14.1, 22,6, 27.3, 29.0, 29.1, 29.3, 31.8, 43.2, 65.9, 108.6108.7, 118.7, 119.5, 120.5, 121.6, 121.8, 122.5, 122.6, 125.7, 126.0, 129.7, 130.7, 135.4, 138.0, 139.4, 140.8, 154.6. HRMS (m/z): [M + H]$^+$ calcd. for C$_{53}$H$_{55}$^{79}Br$_2$N$_2$, 877.2732; found, 877.2726. Anal. Calcd. for C$_{53}$H$_{54}$Br$_2$N$_2$: C, 72.43; H, 6.19; N, 3.19. Found: C, 72.44; H, 5.90; N, 3.43.

2,7-Dibromo-9,9-bis(3-acetyl-9-octylcarbazol-6-yl)-fluorene (4)

Acetyl chloride (0.60 g, 3.69 mmol) was added drop wise to a mixture of **3** (1.50 g, 1.71 mmol) and aluminum chloride (1.37 g, 10.3 mmol) in dry benzene (100 mL) at 25 °C. The reaction mixture was stirred at room temperature for 3 h, and then was poured into water (100 mL) and extracted with ethyl acetate (3 × 50 mL^2). The combined organic layers were dried (MgSO$_4$) and concentrated under reduced pressure. The crude product was recrystallized from ethyl acetate to afford **4** (1.14 g, 69.5%) as yellow crystals. ^{1}H NMR (300 MHz, CDCl$_3$): δ 0.84 (t, J = 6.8 Hz, 6H), 1.32–1.34 (m, 20H), 1.84–1.88 (m, 4H), 2.65 (s, 6H), 4.27 (t, J = 7.2 Hz, 4H), 7.33–7.38 (m, 6H), 7.52 (dd, J = 8.4, 1.5 Hz, 2H), 7.61 (d, J = 1.5 Hz, 2H), 7.67 (d, J = 8.1 Hz, 2H), 7.98 (d, J = 0.9 Hz, 2H), 8.07 (dd, J = 8.7, 1.5 Hz, 2H), 8.55 (d, J = 1.2 Hz, 2H). ^{13}C NMR (75 MHz, CDCl$_3$): δ 14.1, 22.6, 26.7, 27.3, 29.0, 29.1, 29.3, 29.7, 31.7, 43.5, 65.8, 108.3, 109.3, 119.9, 121.8, 121.9, 122.0, 122.4, 123.3, 126.6, 128.7, 129.5, 131.0, 136.7, 138.0, 140.3, 143.6, 154.1, 197.8. HRMS (m/z): [M + H]$^+$ calcd. for C$_{57}$H$_{59}$^{79}Br$_2$N$_2$O$_2$, 961.2943; found, 961.2933. Anal. Calcd. for C$_{57}$H$_{58}$Br$_2$N$_2$O$_2$: C, 71.10; H, 6.07; N, 2.91. Found: C, 70.81; H, 6.06; N, 3.30.

2,7-Dibromo-9,9-bis(3-ethyl-9-octylcarbazol-6-yl)-fluorene (5)

A mixture of **4** (1.13 g, 1.17 mmol), hydrazine (0.56 g, 17.6 mmol), potassium hydroxide (1.20 g, 21.4 mmol), and diethylene glycol (100 mL) was stirred at 190 °C for 12 h under N_2. The cooled mixture was poured into water (200 mL) and extracted with ethyl acetate (3 × 50 mL^2). The organic phases were combined, dried ($MgSO_4$), and concentrated under reduced pressure. The crude product was purified by column chromatography, eluting with hexane/ethyl acetate (1:10), followed by recrystallization from hexane/ethanol to afford **5** (0.50 g, 45.4%) as yellow crystals. ^1H NMR (300 MHz, $CDCl_3$): δ 0.84 (t, J = 6.6 Hz, 6H), 1.23–1.34 (m, 26H), 1.78–1.85 (m, 4H), 2.70–2.78 (q, J = 7.5 Hz, 4H), 4.21 (t, J = 7.2 Hz, 4H), 7.26–7.32 (m, 8H), 7.48 (d, J = 8.3, 1.7 Hz, 2H), 7.61–7.64 (m, 4H), 7.74 (s, 2H), 7.91 (s, 2H). ^{13}C NMR (75 MHz, $CDCl_3$): δ 14.1, 16.6, 22.6, 27.3, 28.9, 29.0, 29.1, 29.4, 31.8, 43.2, 65.9, 108.5, 108.6, 119.3, 119.6, 121.5, 121.8, 122.6, 125.8, 126.0, 129.7, 130.6, 134.8, 135.2, 138.0, 139.3, 139.7, 154.7. HRMS (m/z): $[M + H]^+$ calcd. for $C_{57}H_{63}{}^{79}Br_2N_2$, 933.3358; found, 933.3370. Anal. Calcd. for $C_{57}H_{62}Br_2N_2$: C, 73.23; H, 6.68; N, 3.00. Found: C, 73.30; H, 7.06; N, 3.41.

PF-CBZ-OXD

Aqueous potassium carbonate (2.0 M, 0.8 mL) and Aliquat 336 ($\sim$ 20 mg) were added to a mixture of **5** (60 mg, 64 μmol), **6** (56 mg, 64 μmol), and **7** (82.5 mg, 128 μmol) in toluene (1.5 mL). The mixture was degassed and tetrakis(triphenylphosphine)palladium (5.0 mg, 7.0 mol %) was added in one portion under N_2; the solution was then heated at 110 °C for 36 h. The end groups were capped by heating the mixture under reflux for 12 h with benzeneboronic acid (31.1 mg, 0.25 mmol) and then for 12 h with bromobenzene (40.1 mg, 0.25 mmol). The reaction mixture was cooled to room temperature and precipitated into a mixture of methanol and water (7:3 v/v, 100 mL). The crude polymer was collected, washed with excess methanol, dissolved in THF, and then reprecipitated into methanol. Finally, the polymer was washed with acetone for 48 h using a Soxhlet apparatus and then dried under vacuum to give **PF-CBZ-OXD** (110 mg, 75.6%). ^1H NMR (300 MHz, $CDCl_3$): δ 0.68–0.77 (m, 20H), 0.79–0.82 (m, 6H), 1.00–1.04 (m, 40H), 1.20–1.50 (s, 44H), 1.82–1.98 (m, 12H)

2.71–2.72 (m, 4H), 4.20 (br, 4H), 7.50–7.52 (m, 20H), 7.63–7.92 (m, 20H), 8.00–8.13 (m, 12H). ^{13}C NMR (75 MHz, $CDCl_3$): δ 13.9, 14.0, 14.1, 16.6, 22.5, 22.6, 22.7, 23.8, 27.3, 28.9, 29.1, 29.3, 29.7, 29.9, 30.3, 31.1, 31.6, 31.7, 31.8, 31.9, 35.1, 40.3, 43.2, 55.2, 55.3, 65.8, 66.0, 108.4, 119.3, 119.7, 120.4, 120.8, 121.0, 121.3, 122.5, 122.8, 124.5, 125.1, 125.5, 126.0, 126.5, 126.7, 127.1, 127.2, 127.3, 127.6, 128.3, 128.4, 128.5, 128.7, 128.9, 131.7, 131.9, 132.0, 132.2, 134.7, 136.7, 138.9, 139.2, 139.6, 140.1, 141.1, 141.8, 149.2, 150.7, 151.6, 151.8, 153.9, 155.3, 164.0, 164.7.

Light-Emitting Devices

Polymer LED devices were fabricated in the configuration ITO/poly(styrenesulfonate)-doped poly (3,4-ethylenedioxythiophene) (PEDOT) (35 nm)/ light-emitting layer (50–70 nm)/TPBI (30 nm)/ Mg:Ag (100 nm)/Ag (100 nm). To improve hole injection and substrate smoothness, the PEDOT was spin-coated directly onto the ITO glass and dried at 80 °C for 12 h under vacuum. The light-emitting layer was spin-coated on top of the PEDOT layer, using toluene as the solvent, and then dried under vacuum for 3 h at 60 °C. Prior to casting the film, the polymer solution was filtered through a Teflon filter (0.45 μm). The TPBI layer, which was grown by thermal sublimation in a vacuum of 3×10^{-6} torr, was used as an electron-transport layer that blocked holes and confined excitons. The cathode Mg:Ag (10:1, 100 nm) alloy was deposited onto the TPBI layer through coevaporation of the two metals; an additional layer of Ag (100 nm) was deposited onto the alloy as a protection layer. The current–voltage–luminance characteristics were measured under ambient conditions using a Keithley 2400 source meter and a Newport 1835C optical meter equipped with an 818ST silicon photodiode.

REFERENCES AND NOTES

1. Burroughes, J. H.; Bradley, D. D. C.; Brown, A. R.; Marks, R. N.; Mackay, K.; Friend, R. H.; Burns, P. L; Holmes, A. B. Nature 1990, 347, 539.
2. McGehee, M. D.; Bergstedt, T.; Zhang, C.; Saab, A. P.; O'Regan, M. B.; Bazan, G. C.; Srdanov, V. I.; Heeger, A. J. Adv Mater 1999, 11, 1349.

3. Gong, X.; Robinson, M. R.; Ostrowski, J. C.; Moses, D.; Bazan G. C.; Heeger, A. J. Adv Mater 2002, 14, 581.

4. Kim, J. H.; Herguth, P.; Kang, M.-S.; Jen, A. K.-Y.; Tseng Y.-H.; Shu, C.-F. Appl Phys Lett 2004, 85, 1116.

5. Niu, Y.-H.; Chen, B.; Liu, S.; Yip, H.; Bardecker, J.; Jen, A. K.-Y.; Kavitha, J.; Chi, Y.; Shu, C.-F.; Tseng, Y.-H.; Chien, C.-H. Appl Phys Lett 2004, 85, 1619.

6. Niu, Y.-H.; Tung, Y.-L.; Chi, Y.; Shu, C.-F.; Kim, J. H.; Chen, B.; Luo, J.; Carty, A. J.; Jen, A. K.-Y. Chem Mater 2005, 17, 3532.

7. Wu, F.-I.; Shih, P.-I.; Tseng, Y.-H.; Chen, G.-Y.; Chien C.-H.; Shu, C.-F. J Phys Chem B 2005, 109, 14000.

8. Wu, F.-I.; Shih, P.-I.; Shu, C.-F.; Tung, Y.-L.; Chi, Y. Macromolecules 2005, 38, 9028.

9. Su, H.-J.; Wu, F.-I.; Shu, C.-F.; Tung, Y.-L.; Chi, Y.; Lee, G.-H. J Polym Sci Part A: Polym Chem 2005, 43, 859.

10. King, S. M.; Al-Attar, H. A.; Evans, R. J.; Congreve, A.; Beeby, A.; Monkman, A. P. Adv Funct Mater 2006, 16, 1043.

11. Pei Q.; Yang, Y. J Am Chem Soc 1996, 118, 7416.

12. Neher, D. Macromol Rapid Commun 2001, 22, 1365.

13. Leclerc, M. J Polym Sci Part A: Polym Chem 2001, 39, 2867.

14. Becker, S.; Ego, C.; Grimsdale, A. C.; List, E. J. W.; Marsitzky, D.; Pogantsch, A.; Setayesh, S.; Leising, G.; Müllen, K. Synth Met 2002, 125, 73.

15. Ego, C.; Grimsdale, A. C.; Uckert, F.; Yu, G.; Srdanov, G.; Müllen, K. Adv Mater 2002, 14, 809.

16. Wu, F.-I.; Reddy, D. S.; Shu, C.-F.; Liu, M. S.; Jen, A. K.-Y. Chem Mater 2003, 15, 269.

17. Shu, C.-F.; Dodda, R.; Wu, F.-I.; Liu, M. S.; Jen, A. K.-Y. Macromolecules 2003, 36, 6698.

18. Vak, D.; Shin, S. J.; Yum, J.-H.; Kim, S.-S.; Kim, D.-Y. J Lumin 2005, 115, 109.

19. Tseng, Y.-H.; Shih, P.-I.; Chien, C.-H.; Dixit, A. K.; Shu, C.-F.; Liu, Y.-H.; Lee, G.-H. Macromolecules 2005, 38, 10055.

20. Lee, J.; Cho, H.-J.; Cho, N. S.; Hwang, D.-H.; Kang, J.-M.; Lim, E.; Lee, J.-I.; Shim, H.-K. J Polym Sci Part A: Polym Chem 2006, 44, 2943.

21. Wu, C.-W.; Sung, H.-H.; Lin, H.-C. J Polym Sci Part A: Polym Chem 2006, 44, 6765.

22. Liu, B.; Yu, W.-L.; Lai, Y.-H.; Huang, W. Chem Mater 1984, 2001, 13.

23. Beaupré, S.; Leclerc, M. Adv Funct Mater 2002, 12, 192.

24. Herguth, P.; Jiang, X.; Liu, M. S.; Jen, A. K.-Y. Macromolecules 2002, 35, 6094.

25. Müller, C. D.; Falcou, A.; Reckefuss, N.; Rojahn, M.; Wiederhirn, V.; Rudati, P.; Frohne, H.; Nuyken, O.; Becker, H.; Meerholz, K. Nature 2003, 421, 829.

26. Liu, M. S.; Luo, J.; Jen, A. K.-Y. Chem Mater 2003, 15, 3496.

27. Yang, R.; Tian, R.; Hou, Q.; Yang, W.; Cao, Y. Macromolecules 2003, 36, 7453.

28. Ego, C.; Marsitzky, D.; Becker, S.; Zhang, J.; Grimsdale, A. C.; Müllen, K.; MacKenzie, J. D.; Silva, C.; Friend, R. H. J Am Chem Soc 2003, 125, 437.

29. Chen, X.; Liao, J.-L.; Liang, Y.; Ahmed, M. O.; Tseng, H.-E.; Chen, S.-A. J Am Chem Soc 2003, 125, 636.

30. Yang, J.; Jiang, C.; Zhang, Y.; Yang, R.; Yang, W.; Hou Q.; Cao, Y. Macromolecules 2004, 37, 1211.

31. Su, H.-J.; Wu, F.-I.; Shu, C.-F. Macromolecules 2004, 37, 7197.

32. Su, H.-J.; Wu, F.-I.; Tseng, Y.-H.; Shu, C.-F. Adv Funct Mater 2005, 15, 1209.

33. Yang, R.; Tian, R.; Yan, J.; Zhang, Y.; Yang, J.; Hou, Q.; Yang, W.; Zhang, C.; Cao, Y. Macromolecules 2005, 38, 244.

34. Jiang, J.; Jiang, C.; Yang, W.; Zhen, H.; Huang, F.; Cao, Y. Macromolecules 2005, 38, 4072.

35. Zhen, H.; Luo, C.; Yang, W.; Song, W.; Du, B.; Jiang, J.; Jiang, C.; Zhang, Y.; Cao, Y. Macromolecules 2006, 39, 1693.

36. Cao, D.; Liu, Q.; Zeng, W.; Han, S.; Peng, J.; Liu, S. J Polym Sci Part A: Polym Chem 2006, 44, 2395.

37. Buchgraber, C.; Pogantsch, A.; Kappaun, S.; Spanring, J.; Kern, W. J Polym Sci Part A: Polym Chem 2006, 44, 4317.

38. Jung, Y. K.; Lee, J.; Lee, S. K.; Cho, H.-J.; Shim, H.-K. J Polym Sci Part A: Polym Chem 2006, 44, 4611.

39. Tu, G.; Zhou, Q.; Cheng, Y.; Wang, L.; Ma, D.; Jing, X.; Wang, F. Appl Phys Lett 2004, 85, 2172.

40. Lee, S. K.; Hwang, D.-H.; Jung, B. -J.; Cho, N. S.; Lee, J.; Lee, J.-D.; Shim, H.-K. Adv Funct Mater 2005, 15, 1647.

41. Liu, J.; Zhou, Q. G.; Cheng, Y. X.; Geng, Y. H.; Wang, L. X.; Ma, D. G.; Jing, X. B.; Wang, F. S. Adv Mater 2005, 17, 2974.

42. Tu, G. L.; Mei, C. Y.; Zhou, Q. G.; Cheng, Y. X.; Geng, Y. H.; Wang, L. X.; Ma, D. G.; Jing, X. B.; Wang, F. S. Adv Funct Mater 2006, 16, 101.

43. Jiang, J. X.; Xu, Y. H.; Yang, W.; Guan, R.; Liu, Z. Q.; Zhen, H. Y.; Cao, Y. Adv Mater 2006, 18, 1769.

44. Liu, J.; Zhou, Q. G.; Cheng, Y. X.; Geng, Y. H.; Wang, L. X.; Ma, D. G.; Jing, X. B.; Wang, F. S. Adv Funct Mater 2006, 16, 957.

45. Mitschke, U.; Bäuerle, P. J Mater Chem 2000, 10, 1471.

46. Strohriegl, P.; Grazulevicius, J. V. Adv Mater 2002, 14, 1439.

47. Zhang, Q.; Chen, J.; Cheng, Y.; Wang, L.; Ma, D.; Jing, X.; Wang, F. J Mater Chem 2004, 14, 895.

48. Wu, F.-I.; Shih, P.-I.; Yuan, M.-C.; Dixit, A. K.; Shu, C.-F.; Chung, Z.-M.; Diau, E. W.-G. J Mater Chem 2005, 15, 4753.

49. Li, Y.; Ding, J.; Day, M.; Tao, Y.; Lu, J.; D'iorio, M. Chem Mater 2004, 16, 2165.

50. Du, J.; Fang, Q.; Bu, D.; Ren, S.; Cao, A.; Chen, X. Macromol Rapid Commun 2005, 26, 1651.

51. Jin, Y.; Kim, J. Y.; Park, S. H.; Kim, J.; Lee, S.; Lee, K.; Suh, H. Polymer 2005, 46, 12158.

52. Wu, C.-W.; Tsai, C.-M.; Lin, H.-C. Macromolecules 2006, 39, 4298.

53. Grigalevicius, S.; Ma, L.; Xie, Z.-Y.; Scherf, U. J Polym Sci Part A: Polym Chem 2006, 44, 5987.

54. Shih, P.-I.; Chiang, C.-L.; Dixit, A. K.; Chen, C.-K.; Yuan, M.-C.; Lee, R.-Y.; Chen, C.-T.; Diau, E. W.-G.; Shu, C.-F. Org Lett 2006, 8, 2799.

55. Brunner, K.; van Dijken, A.; Börner, H.; Bastiaansen, J. J. A. M.; Kiggen, N. M. M.; Langeveld, B. M. W. J Am Chem Soc 2004, 126, 6035.

56. Kulkarni, A. P.; Zhu, Y.; Jenekhe, S. A. Macromolecules 2005, 38, 1553.

57. Eaton, D. F. Pure Appl Chem 1988, 60, 1107.

58. List, E. J. W.; Guentner, R.; de Freitas, P. S.; Scherf, U. Adv Mater 2002, 14, 374.

59. Gaal, M.; List, E. J. W.; Scherf, U. Macromolecules 2003, 36, 4236.

60. Zeng, G.; Yu, W.-L.; Chua, S.-J.; Huang, W. Macromolecules 2002, 35, 6907.

61. Grice, A. W.; Bradley, D. D. C.; Bernius, M. T.; Inbasekaran, M.; Wu, W. W.; Woo, E. P. Appl Phys Lett 1998, 73, 629.

62. Chou, C.-H.; Hsu, S.-L.; Dinakaran, K.; Chiu, M.-Y.; Wei, K.-H. Macromolecules 2005, 38, 745.

63. Chien, C.-H.; Shih, P.-I.; Wu, F.-I.; Shu, C.-F.; Chi, Y. J Polym Sci Part A: Polym Chem 2007, 45, 2073.

64. Wu, F.-I.; Su, H.-J.; Shu, C.-F.; Luo, L.; Diau, W.-G.; Cheng, C.-H.; Duan, J.-P.; Lee, G.-H. J Mater Chem 2005, 15, 1035.

65. Chen, F.-C.; Chang, S.-C.; He, G.; Pyo, S.; Yang, Y.; Kurotaki, M.; Kido, J. J Polym Sci Part B: Polym Phys 2003, 41, 2681.

66. Uchida, M.; Adachi, C.; Koyama, T.; Taniguchi, Y. J Appl Phys 1999, 86, 1680.

67. Ranger, M.; Leclerc, M. Can J Chem 1998, 76, 1571.

68. Ranger, M.; Rondeau, D.; Leclerc, M. Macromolecules 1997, 30, 7686.